3341
P.34

# NASA
# Technical
# Memorandum

NASA TM - 103528

# GEOSIM - A NUMERICAL MODEL FOR GEOPHYSICAL
# FLUID FLOW SIMULATION

By Karen A. Butler, Timothy L. Miller,
and Huei-Iin Lu

Space Science Laboratory
Science and Engineering Directorate

February 1991

# NASA

National Aeronautics and
Space Administration

**George C. Marshall Space Flight Center**

MSFC - Form 3190 (Rev. May 1983)

# Report Documentation Page

| 1. Report No. NASA TM - 103528 | 2. Government Accession No. | 3. Recipient's Catalog No. |
|---|---|---|

| 4. Title and Subtitle GEOSIM - A Numerical Model for Geophysical Fluid Flow Simulation | 5. Report Date February 1991 |
|---|---|
| | 6. Performing Organization Code ES42 |

| 7. Author(s) Karen A. Butler,[*] Timothy L. Miller, and Huei-Iin Lu[**] | 8. Performing Organization Report No. |
|---|---|
| | 10. Work Unit No. |

| 9. Performing Organization Name and Address George C. Marshall Space Flight Center Marshall Space Flight Center, AL 35812 | 11. Contract or Grant No. |
|---|---|
| | 13. Type of Report and Period Covered Technical Memorandum |

| 12. Sponsoring Agency Name and Address National Aeronautics and Space Administration Washington, D.C. 20546 | 14. Sponsoring Agency Code |
|---|---|

16. Abstract

A numerical model which simulates geophysical fluid flow in a wide range of problems is described in detail, and comparisons of some of the model's results are made with previous experimental and numerical studies. The model is based upon the Boussinesq Navier-Stokes equations in spherical coordinates, which can be reduced to a cylindrical system when latitudinal walls are used near the pole and the ratio of latitudinal length to the radius of the sphere is small. The equations are approximated by finite differences in the meridional plane and spectral decomposition in the azimuthal direction. The user can specify a variety of boundary and initial conditions, and there are five different spectral truncation options. The results of five validation cases are presented: (1) the transition between axisymmetric flow and baroclinic wave flow in the side-heated annulus; (2) the steady baroclinic wave of the side-heated annulus; (3) the wave-amplitude vacillation of the side-heated annulus; (4) transition to baroclinic wave flow in a bottom-heated annulus; and (5) the Spacelab Geophysical Fluid Flow Cell (spherical) experiment.

| 17. Key Words (Suggested by Author(s)) Numerical Model, Geophysical Fluid Dynamics, Finite Difference | 18. Distribution Statement Unclassified--Unlimited |
|---|---|

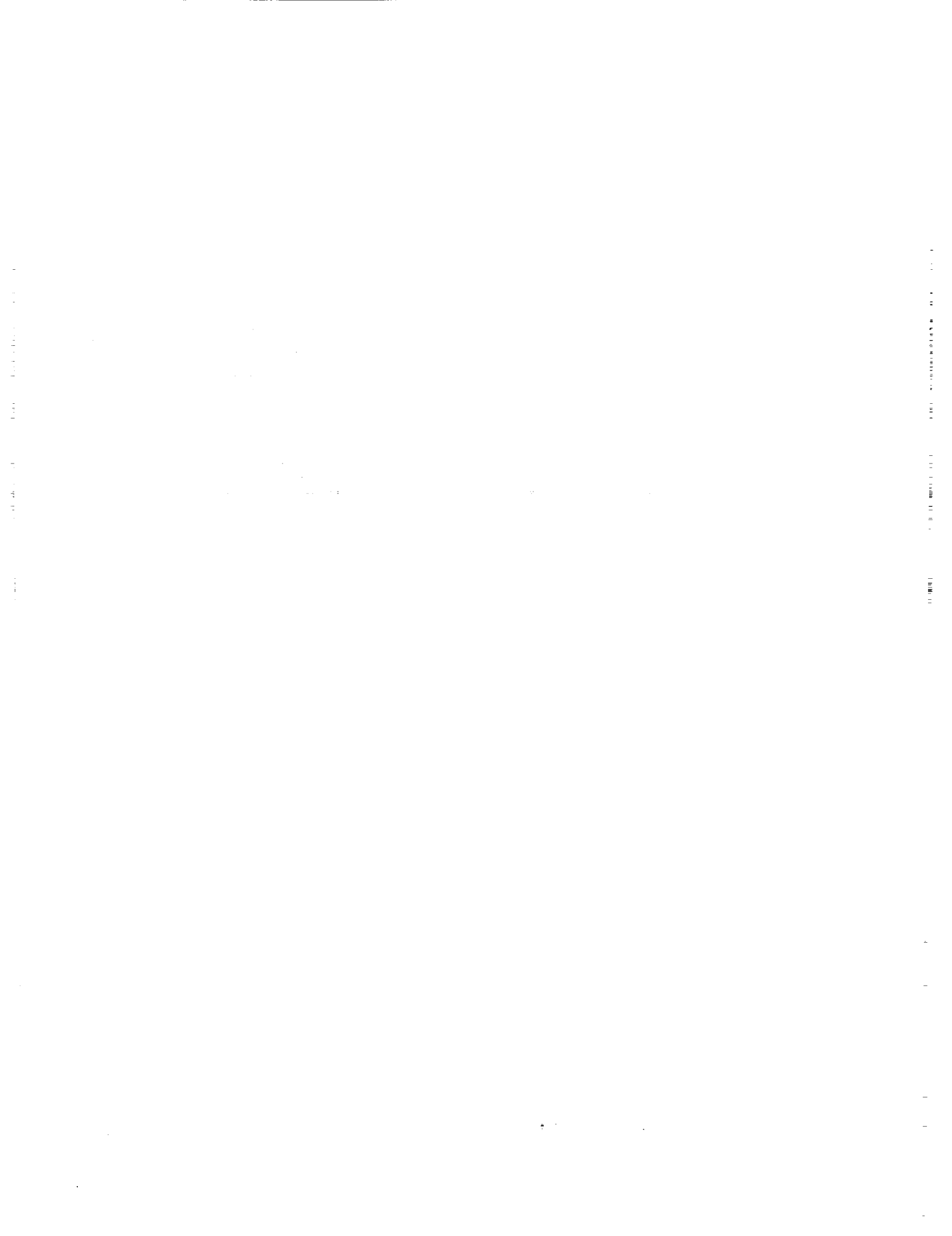| 19. Security Classif. (of this report) Unclassified | 20. Security Classif. (of this page) Unclassified | 21. No. of pages 37 | 22. Price NTIS |
|---|---|---|---|

# TABLE OF CONTENTS

# LIST OF ILLUSTRATIONS

# LIST OF TABLES

# I. INTRODUCTION

There have been many studies of geophysical fluid dynamics that deal with flow under the combined influence of buoyancy and rotation. The flows which are seen in cylindrical annulus experiments in which the thermal forcing and the rate of rotation are varied [1,2] range from simple axisymmetric flows to a full spectrum of waves interacting in a chaotic fashion. In a hemispherical shell space-laboratory experiment, Hart et al. [3] found a wide range of flow regimes depending upon the heating configuration and rotation rate. Such experiments are aimed at enhancing our understanding of atmospheric and oceanic dynamics by studying controlled, simple systems in which the flow dynamics can be isolated. However, any experiments are subject to instrumentation errors that affect the fidelity of the controlled conditions and to the data acquisition difficulties that prohibit detailed analyses of the phenomona under investigation, as well as to the expensive cost that discourages systematic and wider range parametric studies. A carefully developed numerical model that can simulate the experiments is a viable approach to the solutions of these problems. This approach allows more accurate control on the experimental conditions. It provides a complete data source for performing diagnostic studies. It can cost very little to run a high resolution model on a supercomputer if the model is coded efficiently. Our objective has been to develop an effective model that is able to simulate a broad range of configurations, including those mentioned above.

The purpose of this paper is to describe the GEOSIM (geophysical fluid flow simulation) model which has recently been developed at the Marshall Space Flight Center (MSFC). It is a result of extensive renovation and expansion of the model used by Miller and Gall [4,5]. The model has been validated by comparing its results with those of laboratory experiments and other numerical models. Miller and Butler [6] and Miller and Fehribach [7] have given recent reports on the use of this model, although their papers use only part of the full capability of the model. In this paper, we present other validation results which are of interest to the community. These cases are: (1) the steady baroclinic wave in a rotating side-heated annulus [8], (2) the amplitude vacillation studies of Buzyna et al. [9], (3) transition to baroclinic waves in the bottom-heated annulus.experiments at MSFC [10], and (4) the Spacelab Geophysical Fluid Flow Cell (GFFC) observations described by Hart et al. [3].

# II. DESCRIPTION OF THE MODEL

## A. Equations

The model is based upon the Boussinesq Navier-Stokes equations in rotating spherical coordinates. The equations, with the advective terms written in flux form, are as follows. The definitions of the symbols are given in Table 1.

## Table 1. List of Symbols.

| | |
|---|---|
| $a$ | Inner radius |
| $d$ | Depth |
| $g$ | Body force ("gravity") |
| $g_o$ | Gravity at $r = a$ |
| $k$ | Longitudinal wavenumber |
| $P$ | Pressure |
| $r$ | Radial coordinate, distance from center |
| $t$ | Time |
| $T$ | Temperature |
| $u$ | Longitudinal velocity (positive for westerly flow) |
| $v$ | Meridional velocity (positive for southerly flow) |
| $w$ | Radial velocity |
| $\beta$ | Thermal expansivity |
| $\phi$ | Latitudinal coordinate |
| $\kappa$ | Thermal diffusivity |
| $\lambda$ | Longitudinal coordinate |
| $\Pi$ | $P/\rho_o$ (often referred to a "pressure" in text) |
| $\rho_o$ | Reference density |
| $\nu$ | Kinematic viscosity |
| $\Omega$ | Rotation rate |

$$\frac{\partial u}{\partial t} = -\left(\frac{1}{r\cos\phi}\frac{\partial}{\partial\phi}(uv\cos\phi) + \frac{1}{r^2}\frac{\partial}{\partial r}(wur^2) + \frac{1}{r\cos\phi}\frac{\partial u^2}{\partial\lambda}\right) + \frac{uv\tan\phi}{r} - \frac{uw}{r} + 2\Omega v\sin\phi$$

$$-2\Omega w\cos\phi + \nu\left[\nabla^2 u - \frac{1}{r^2\cos^2\phi}\left(u + 2\frac{\partial}{\partial\lambda}(v\sin\phi - w\cos\phi)\right)\right] - \frac{1}{r\cos\phi}\frac{\partial\Pi}{\partial\lambda}.$$

$$\tag{1}$$

$$\frac{\partial v}{\partial t} = -\left(\frac{1}{r\cos\phi}\frac{\partial}{\partial\phi}(v^2\cos\phi) + \frac{1}{r^2}\frac{\partial}{\partial r}(wvr^2) + \frac{1}{r\cos\phi}\frac{\partial uv}{\partial\lambda}\right) - \frac{u\tan\phi}{r} - \frac{vw}{r}$$

$$-2\Omega u\sin\phi + \nu\left[\nabla^2 v - \frac{v}{r^2\cos^2\phi} + \frac{2\sin\phi}{r^2\cos^2\phi}\frac{\partial u}{\partial\lambda} + \frac{2}{r^2}\frac{\partial w}{\partial\phi}\right] - \frac{1}{r}\frac{\partial\Pi}{\partial\phi}.$$

$$\tag{2}$$

$$\frac{\partial w}{\partial t} = -\left(\frac{1}{r\cos\phi}\frac{\partial}{\partial\phi}(vw\cos\phi) + \frac{1}{r^2}\frac{\partial}{\partial r}(w^2 r^2) + \frac{1}{r\cos\phi}\frac{\partial uw}{\partial\lambda}\right) + \frac{(u^2 + v^2)}{r}$$

$$+2\Omega u\cos\phi + \nu\left[\nabla^2 w - \frac{2}{r^2\cos\phi}\frac{\partial}{\partial\phi}(v\cos\phi) - \frac{2}{r^2\cos\phi}\frac{\partial u}{\partial\lambda} - \frac{2w}{r^2}\right] + \beta gT - \frac{\partial\Pi}{\partial r}.$$

$$\tag{3}$$

$$\frac{\partial T}{\partial t} = -\left(\frac{1}{r\cos\phi}\frac{\partial}{\partial\phi}(vT\cos\phi) + \frac{1}{r^2}\frac{\partial}{\partial r}(wTr^2) + \frac{1}{r\cos\phi}\frac{\partial uT}{\partial\lambda}\right) + \kappa(\nabla^2 T) .$$

$$\tag{4}$$

The continuity equation is as follows:.

$$\frac{1}{r\cos\phi}\frac{\partial}{\partial\phi}(v\cos\phi) + \frac{1}{r^2}\frac{\partial}{\partial r}(wr^2) + \frac{1}{r\cos\phi}\frac{\partial u}{\partial\lambda} = 0 .$$

$$\tag{5}$$

The spherical three-dimensional Laplacian is:

$$\nabla^2\gamma \equiv \frac{1}{r^2\cos^2\phi}\frac{\partial\gamma^2}{\partial\lambda^2} + \frac{1}{r^2\cos\phi}\frac{\partial}{\partial\phi}\left(\cos\phi\frac{\partial\gamma}{\partial\phi}\right) + \frac{1}{r^2}\frac{\partial}{\partial r}\left(r^2\frac{\partial\gamma}{\partial r}\right).$$

$$\tag{6}$$

### B. Numerical Method

The model uses a mixed spectral and finite difference technique, similar to that used by Quon [11] for a cylindrical model. In the azimuthal direction, each field is decomposed into Fourier components of the form $A_k\exp(ik\lambda)$, where $\lambda$ is longitude, $k$ is a given wavenumber (0 for axisymmetric), and $A_k$ is the complex amplitude of one of the dependent variables. By substituting the Fourier series for each variable into equations (1)-(4) and operating on both sides

by the orthogonalization procedure, one obtains a set of equations for each Fourier mode [11]. These equations can be simplified in a consistent manner to represent various mathematical systems in different degrees of complexity. GEOSIM is able to solve five classes of problems, which are handled consistently with the same numerical algorithms:

1. Axisymmetric flow

2. Linear instability problem with respect to a previously computed, fixed axisymmetric state

3. Linear instability problem with respect to an evolving axisymmetric state as in 1.

4. Nonlinear problem for single and multiple waves, in which the only quadratic terms retained are those due to the interaction between the wave and axisymmetric parts of the flow (hereafter called the wave-mean flow interaction case)

5. Fully nonlinear problem for multiple waves with complete wave-mean and wave-wave interactions.

Note that modes 2 and 3 compute wave structure and its corresponding growth rate which asymptotically becomes the fastest among the modes of the linear system. The detail of computing the eigenfunction and the eigenvalue is given in the next paragraph. Mode 4 allows an arbitrary sequence of wavenumbers in the model. Mode 5 deals with a simple spectral truncation series with wavenumber being multiplied by a fixed harmonic factor. Therefore, in addition to the traditional spectral resolution 1 to K, the model can solve for the same number of wave components but in a higher harmonic, e.g., wavenumbers 2, 4, ..., 2K. In mode 5 application, the well-known transform method (see ref. [12]) is employed to compute the spectral transformations of nonlinear terms in the equations. Details of this method are given in section II.F.

The method of computing the largest real eigenvalue and its associated eigenfunction deserves special attention. The model is integrated forward in time in the expectation that the solution will eventually become dominated by the fastest-growing (or slowest-decaying) eigenmode. At each time step an estimate of the linear, complex growth rate ($\omega$) is calculated for the wave by spatially integrating the temperature tendency terms. The term ($-\omega Q$) is added to each of the wave prognostic equations (where $Q$ refers to the prognostic variable). If the fields become dominated by a single fastest-growing (or slowest-decaying) eigenmode, this additional term stops the wave from growing (or decaying) and propagating. For most situations, this indeed occurs, and the system of equations (with the additional term $-\omega Q$) has a steady state solution. The use of this technique avoids the situation of the model "blowing up" due to exponential growth, it makes the solution independent of the time-stepping formulation, and it allows the use of differential time steps to enhance the convergence rate.

4

A similar procedure can be applied as an option to obtain a steady state solution for the mode 4 application when the solution includes a wave of constant structure which propagates azimuthally. In that case, only the imaginary part of the growth rate is used in the additional term. After a steady wave is achieved in the solution, this procedure stops the wave from propagating in the azimuthal direction and permits the calculation of a time-independent solution.

In the cases in options (1) through (4) where the steady state is the desired result, the use of differential time steps (different values of the time step for different equations) can dramatically speed up the rate of convergence. In particular, this is true for cases in which either momentum or heat (usually the latter) has a much lower diffusivity than the other. The time step constraint in the cases of interest is often due to the diffusive terms; hence, the time step for the more slowly diffusing component can be made several times that of the other component without loss of numerical stability or accuracy (for steady state flows). Of course, variable time steps are never used in cases where the time evolution is important (for example, vacillation studies).

## C. Spatial Discretization

1. <u>The Grid System</u>. The model uses a staggered grid system (see Figure 1) similar to that of Quon [11]. The physical domain is partitioned into an arrangement of J by K (JJ-2 by KK-2, in the code's nomenclature) elements in the meridional and vertical directions. The variables $u$, $T$, and $\Pi$ are defined in the center of the elements; $v$ is defined at the middle of the vertical boundary of each element (i.e., on the sides); and $w$ is defined at the middle of the top and bottom of each element. Note that the grid system includes artificial points outside the physical domain, for efficiency in computation and accuracy in imposing the boundary conditions. The grid can be stretched in both directions, so that finer resolution can be obtained in regions of strong gradients. The initialization routine of the model constructs a stretched grid which has grid spacings that are determined based on the formula $\sin(\pi\gamma) + \delta$, where $\gamma$ ranges from zero to one (proportional to physical distance) and $\delta$ is an input parameter. For larger $\delta$ the grid stretching is less severe. There is also an input parameter which adjusts the location where the grid is to be stretched. This is done by moving the sine function so that the desired amount of stretching in the location of interest is achieved. After the spacing function is determined, the grid intervals are multiplied by the appropriate constant such that they are in the proper units. The method differs from that of Quon, who transforms the equations to a stretched coordinate system and then discretizes with a constant interval. The advantage of the current method is to achieve increased flexibility, which is important because of the requirement to use the same model for a variety of geometries and flow types.

2. <u>Finite Differencing</u>. The spatial derivatives in the Fourier transformed equations are approximated by a control volume discretization procedure. Standard centered difference approximations are used for the derivatives in each of the equations with the following exceptions.

For the temperature equation, the terms representing advection of heat by the mean meridional flow are evaluated as a weighted average of upwind and centered differences. The

u    v    u    v    u    v    u

w       w       w       w

$r \uparrow$

u    v    u    v    u    v    u

w       w       w       w

u    v    u    v    u    v    u

w    w       w       w

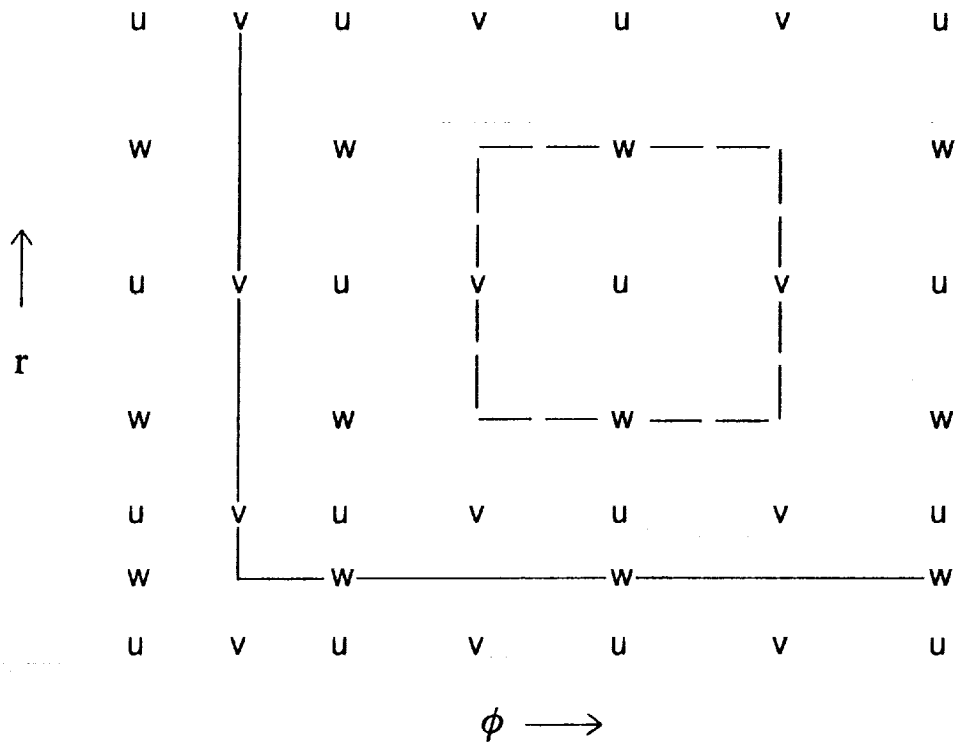u    v    u    v    u    v    u

$\phi \longrightarrow$

Figure 1. Staggered grid system, showing the placement of the velocity components. The $T$ and $\Pi$ variables are placed on the same points as the $u$ component.

relative weights given to the two differences is input by the user. A heavier weight on the upwind scheme may help suppress oscillatory behavior of the numerical solution due to the splitting property inherent in the centered differencing scheme. However, too much upwind differencing introduces artificial viscosity (see ref. [13]), which may degrade the accuracy of the solution. Thus, the requirements for upwind differencing must be evaluated for each individual problem. In general, we have used upwind differencing as little as possible, introducing the smallest fraction necessary to avoid small-scale features which are clearly numerical (which occur due to the advective time scale becoming smaller than the diffusive time scale).

The second exception to the standard centered differencing formulation deals with the evaluation of the flux terms in the $v$ and $w$ equations. In that case, the Warn-Varnas et al. [14] "Scheme B" is used in order to conserve kinetic energy while retaining second order accuracy.

<div align="center">D. Time Discretization</div>

A two-level scheme is used for the time differencing, which minimizes the computer memory requirements. First-order forward differencing is generally used, although exceptions to this rule are made according to numerical stability criteria. Those deviations are described in the following paragraphs.

In order to lessen the time step constraint due to the presense of inertial gravity waves, the Coriolis and the body force terms in the $w$ and $v$ equations use newly updated values of $u$ and $T$ (i.e., $u$ and $T$ are updated first, before the tendencies of $v$ and $w$ are calculated). While this introduces no complication for the axisymmetric part of the flow where $u$ is not involved in the continuity equation, mass continuity requires that all three velocity components be updated simultaneously in the wave equations. In the latter case, a tentative value of $u$, based upon the pressure at the previous time step, is used in the Coriolis terms for $v$ and $w$. Experience has shown that the difference in the results obtained between this update procedure and the standard forward differencing scheme is insignificant, while the gain in allowable time can be sizable when the rotation rate or the vertical stratification is large.

To further permit longer time steps, there is an ADI (alternating direction implicit) option for the diffusion terms and those involving advection by the mean flow. The ADI method treats terms implicitly in one direction and explicitly in the other direction for even time steps, and on the odd time steps switches directions. The following is a description of the ADI method applied to the vertical direction at odd time steps, using the $T$ equation as an example. Letting $n+1$ and $n$ be the forecast and current time levels, respectively, the equation is discretized as follows:

$$\frac{\partial T}{\partial t} \approx \delta_t \equiv \frac{\Delta T}{\Delta t} = \frac{T^{n+1} - T^n}{\Delta t} = -(D_r T^{n+1} + D_\phi T^n + D_\lambda T^n) + \kappa(L_r^2 T^{n+1} + L_\phi^2 T^n + L_\lambda^2 T^{n+1}), \qquad (7)$$

where $D_\lambda$, $D_\phi$, and $D_r$ represent the centered finite difference approximation of flux divergences due the axisymmetric components of $u$, $v$, and $w$, respectively, and the $L^2$'s represent the finite difference analog to the Laplacian components. The velocity components (valid at time level n)

<div align="center">7</div>

are included in our definition of the operator $D$. The equations are rewritten in terms of $\Delta T$ and $T^n$. This is done by adding and subtracting the terms on the right-hand side that are at time step n, then replacing $(T^{n+1} - T^n)$ with $\Delta T$ and gathering all the terms involving $\Delta T$ on the left-hand side:

$$\left[1 - \Delta t \left(\kappa\left(L_r^2 + L_\lambda^2\right)\right) - D_r\right] \Delta T = \text{discretized form of the} \tag{8}$$

<div align="center">right-hand side of (4)</div>

<div align="center">involving values at time step n.</div>

When (8) is expanded into matrix form, it is a tridiagonal matrix system for $\Delta T$ and is solved by Gaussian elimination. At even time steps, the $r$-derivatives on the left-hand side are replaced by the $\phi$-derivatives. Note that the $\lambda$ part of the diffusion is implicit and the $\lambda$ part of the advection is explicit at all time steps.

<div align="center">E. Poisson Equation for Pressure</div>

At each time step, a pressure field must be found which results in mass continuity (zero divergence) for the new velocity field. The procedure is similar to that of Williams [15]. A Poisson equation is derived by first writing equations (1)-(3) in vector form:

$$\frac{\partial V}{\partial t} = -\nabla\Pi + G, \tag{9}$$

where $V$ is the velocity vector and $G$ represents the terms on the right-hand sides of equations (1)-(3) other than the pressure gradient terms.

Replacing the left-hand side of (9) by forward differences and multiplying both sides by $\Delta t$ gives:

$$V^{n+1} - V^n = -(\nabla\Pi^* + G^*)\, \Delta t. \tag{10}$$

$\Pi^*$ is the change in pressure from the previous time step and the gradient of the old $\Pi$ is included in the definition of $G^*$. Applying the divergence operator on (10), setting the divergence of the new velocity vector to zero, and rearranging terms gives:

$$\nabla^2\Pi^* = \frac{\nabla \cdot (V^n + G^*\Delta t)}{\Delta t}. \tag{11}$$

Note that the term $\nabla \cdot V^n$ is kept on the right-hand side since there is some round-off divergence from the previous time step. The boundary condition used is that the normal derivative of $\Pi^*$ is zero. This is consistent with our formulation of the Laplacian, in which the normal derivative across the boundary is taken to be zero (justifiable because the momentum equation is not used to

predict the boundary values). As explained by Williams [15], this condition results in $\Pi^*$ being actually a quantity equal to the physical pressure correction except at the boundaries. A correction to $\Pi^*$ could then be applied in order to recover the physical quantity; however, that step is not necessary, since the boundary derivative of $\Pi$ is not required in solving the momentum equations. The elliptic equation with the Neumann boundary condition is solved using a direct method that is vectorized for the CRAY-XMP [16]. The solver has no problem with the fact that there is not a unique solution for the axisymmetric part. It should be noted that the solution of the pressure equation is the most time consuming part of the model. For this reason, we provide a control that skips the pressure update if the maximum absolute value of the divergence is smaller than a prescribed value.

## F. FFT - Method for Solving for Nonlinear Terms

Around an azimuthal ring, every dependent variable is expanded in a discrete complex Fourier series as follows:

$$q(\lambda_j) = \sum_{k=-K}^{K} Q_k \exp(\lambda_j), \tag{12}$$

where $\lambda_j = 2\pi j/L$, $L$ is the number of intervals in the azimuthal direction, and $K$ is the truncation limit of wavenumber $k$. The Fourier (or spectral) coefficients, $Q_k(r,\phi,t)$, are computed by the following:

$$Q_k = \frac{1}{L} = \sum_{j=1}^{L} q(\lambda_j) \exp(ik\lambda_j). \tag{13}$$

Note that (13) is exact only if the product $q(\lambda_j)\exp(ik\lambda_j)$ is a truncated.trigonometric series with maximum wavenumber less than or equal to $L$-1. Otherwise, aliases would result. Hence, if $q(\lambda_j)$ represents a product of two real variables representable by the same spectral series with truncation '$K$, then $L \geq 3K+1$ must be satisfied. The actual calculations of (12) and (13) are carried out by a vectorized fast Fourier transform (FFT) algorithm [17]. This FFT is the same as that used by the NCAR Community Climate Model which limits $L$ to have multiplication factors of 2, 3, and 5 only. This does not place a constraint upon $K$, although since optimal values for $L$ as a function of the number of waves are tabulated in the present program, the number of waves must be $\leq 40$. This number can easily be increased by expanding the table.

Since $q(\lambda_j)$ is real, the complex discrete Fourier transform is conjugate symmetric; i.e., $Q_k = Q^*_{-k}$. Hence, only $k = 0$ to $K$ Fourier coefficients are calculated. In fact, (12) and (13) can be rewritten in a real trigonometric form as follows:

$$q(\lambda_j) \frac{1}{2} a_0 + \sum_{k=1}^{K} (a_k \cos k\lambda_j + b_k \sin \lambda_j), \tag{14}$$

9

where

$$a_k = \frac{2}{L} \sum_{j=1}^{L} q(\lambda_j) \cos k\lambda_j \tag{15}$$

$$b_k = \frac{2}{L} \sum_{j=1}^{L} q(\lambda_j) \sin k\lambda_j. \tag{16}$$

Hence, for each complex coefficient, $Q_k$, the real and imaginary parts are one half of the coefficients of cosine and sine series, except for the $k = 0$ component. The Fourier transform method described above (see also ref. [12]) is efficient in dealing with the nonlinear (quadratic) terms in the governing equations (1)-(4). In short, all variables required in the calculations are first synthesized into physical space, where the quadratic factors (e.g., $uv$, $v^2$, $vT$, etc.) in the nonlinear terms are calculated. The spectral coefficients of those terms are calculated using the FFT. These spectral coefficients are then used in the finite differencing scheme to obtain the nonlinear tendencies for each wave component. Note that the FFT is used only when a fully nonlinear run of the model is made (mode 5). Otherwise, the nonlinear terms (which do not involve wave-wave interactions) are calculated in spectral space, on the $r$-$\phi$ grid.

## G. Boundary Conditions

The model fluid is confined in a latitudinal channel of arbitrary width (which may include the pole as part of the fluid domain) and depth around the polar axis. The use of latitudinal walls at any latitude is an advantage of the hybrid scheme; this would not be possible if, for instance, spherical harmonics were used. Each of the four computational boundaries has the option of being free-slip (zero stress) or no-slip (zero velocity), and each boundary may have a heated (fixed temperature) or adiabatic (zero normal gradient) temperature boundary condition. The temperature profile imposed upon a differentially heated horizontal boundary can have a linear, sine, or logarithmic shape, where the latter is defined by Equation (7) in Miller and Fehribach [7]. The vertical boundaries for the temperature have a linear profile. It is straightforward for a user to program a different temperature profile. The values of vertical velocity ($w$) on the top and bottom are set to zero regardless of the boundary condition configuration. The value of the $v$-component is set to zero on the two meridional boundaries, except for the case in which the domain extends to the pole (next paragraph).

Polar Cases. When there is a pole in the domain (e.g., a full cylinder or spherical shell), the computional boundary condition there is non-trivial. The pole is a singular point in the coordinate system (i.e., the velocity components are not well defined there), but there are no physical constraints on the flow. Fortunately, the grid is structured such that a polar boundary condition is required only for the $v$-component of velocity. The values for the other variables are arbitrary because they are always multiplied by zero in the finite difference scheme. This is due to the fact that the differences are in flux form and the area of the pole itself is zero. However, the polar value of $v$ is used in the calculation of viscous stress one-half grid interval from the pole in order to calculate the viscous tendency for $v$ at the point one grid interval from the pole. By

considering a small neighborhood of the pole, it may be easily shown that the only Fourier component which includes non-zero flow at the pole is the wavenumber one component. Therefore, a correct condition for the axisymmetric and all wave components except wavenumber one is to set $v$ zero at the pole. For the wavenumber one component, the correct boundary condition is zero meridional gradient. This arises from the fact that the flow resulting from the wavenumber one component along a great circle passing through the pole must be symmetric about the pole and must have a finite (Cartesian) derivative at the pole. This derivative is approximated by setting the polar value equal to that one grid point from the pole, which is only first-order accurate.

To produce smooth cross-section plots, polar values of the other components are needed when plotting. A zero meridional gradient is used for the axisymmetric components of $w$ and $T$, and zero amplitude values are used for the wave components. The boundary condition on $u$ is taken to be the same as for $v$.

## III. MODEL VALIDATION

### A. Axisymmetric Flow, Linear Waves, and Hysteresis

Verification of the model was performed in the order of complexity of the problem. Axisymmetric results were compared and agree well with previous results by Williams [8], Quon [11], and Miller and Gall [4,5]. (Note that, while the computer code was rewritten, there was no fundamental change in the algorithm for the axisymmetric case from the Miller and Gall papers ). Linear wave results were compared with Miller and Gall [5]. Exact agreement in the latter case was not obtained nor expected, since the Miller and Gall model made the hydrostatic assumption in the wave component of the flow. The next step was to verify the model with the addition of the nonlinear wave-mean flow terms. Miller and Butler [6] used the model in mode 4 to calculate hysteresis in the transition curve as found experimentally by Fein [1], and good agreement with the experiment was obtained, as shown in Figure 2.

### B. Steady Baroclinic Annulus Wave: Comparison with Previous Work

Attempts were made to validate a steady wave case with Williams [8] and Quon [11]. Note that Quon's model is essentially the same as our model in the single wave-mean flow interaction mode, while William's model is similar to our model in a multiple wave, fully nonlinear mode. With the periodicity condition applied to one-fifth of the annulus, the wave components resolvable in the Williams model are 5, 10, 15, etc. Figure 3 shows the azimuthal mean state from the GEOSIM model in mode 4, including only wavenumber 5. In comparison with the Quon and Williams results (which share resemblance), the wave has smaller amplitude and the mean fields are not affected as much by feedback from the wave. However, the differences reduced considerably when the model was run in fully nonlinear mode with waves 5 and 10 included. When wave 15 was also included (Figure 4), we obtained results that virtually agreed with those of Quon and Williams. We also ran GEOSIM in single-wave mode with wave 4 instead of wave 5 selected, and found that the resultant axisymmetric state and wave amplitude
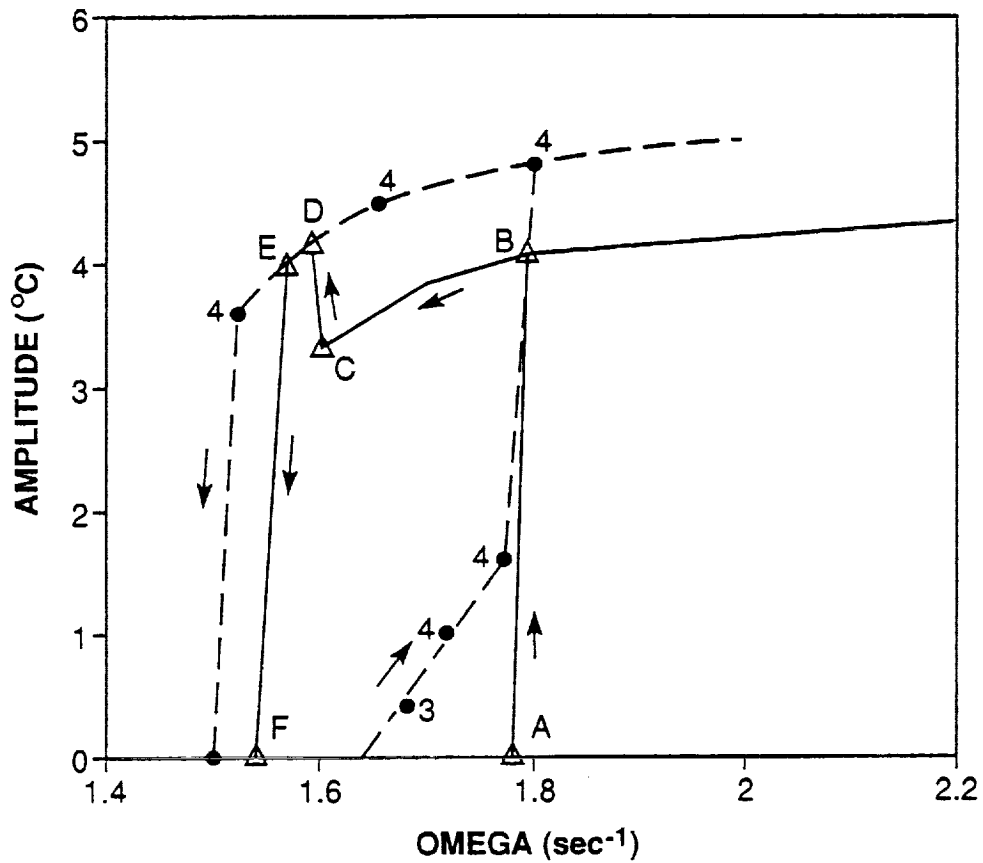
11

Figure 2. Amplitude of the temperature wave as a function of rotation rate as determined by Fein [1] (dashed curve) and Miller and Butler [6]. As the rotation is increased with an axisymmetric state established, the model predicts transition to baroclinic wave flow at point A. As the rotation rate is decreased with a wave established, the model predicts transition to axisymmetric flow at point F.
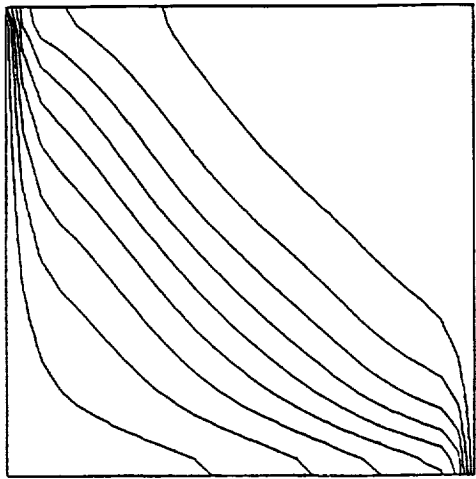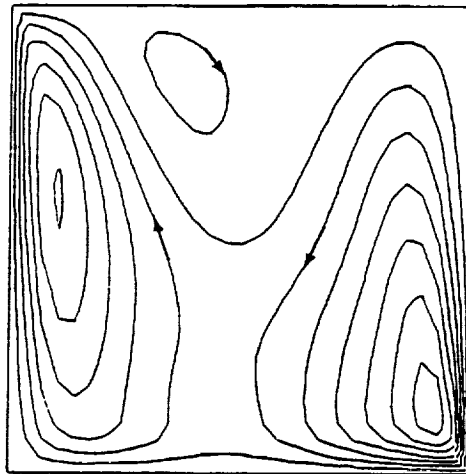
Temperature
Contour Interval = 0.5

Mean State
Maximum = 5.0
Minimum = 0.0
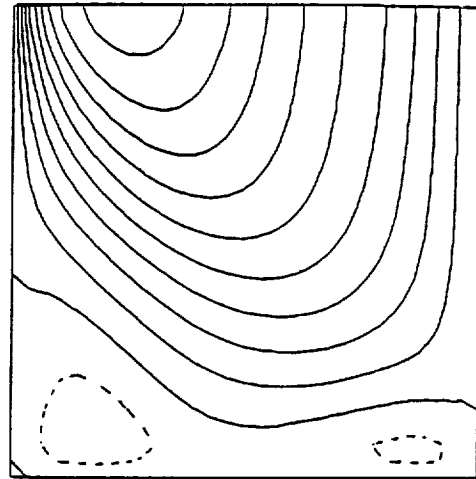
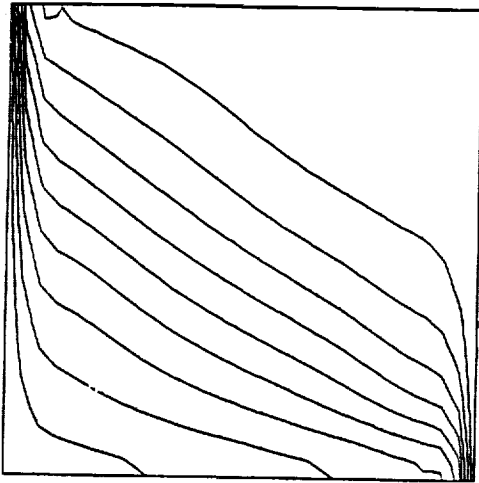Zonal Velocity
Contour Interval = 0.05

Mean State
Maximum = 0.476
Minimum = -0.082

Stream Function
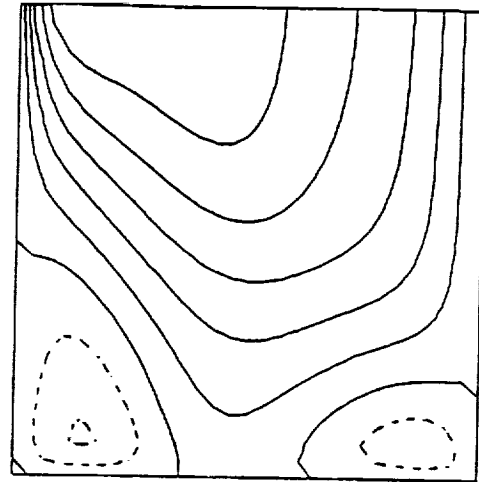Contour Interval = 0.005

Mean State
Maximum = 0.038
Minimum = -0.0007

Figure 3. Temperature, zonal velocity, and meridional stream function from the azimuthal mean state computed by GEOSIM in mode 4 for the case of Williams [8] when a single wave (5) is used.
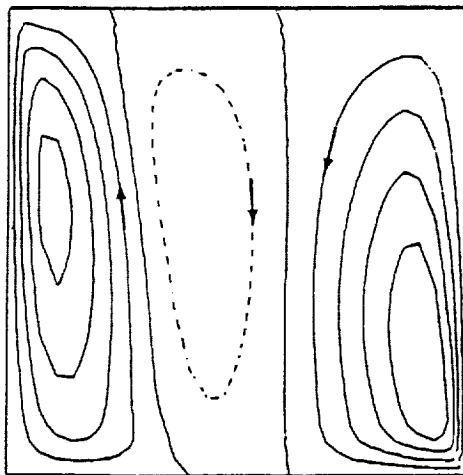
Temperature
Contour Interval = 0.5

Mean State
Maximum = 5.0
Minimum = 0.0

Zonal Velocity
Contour Interval = 0.05

Mean State
Maximum = 0.291
Minimum = -0.105

Stream Function
Contour Interval = 0.01

Mean State
Maximum = 0.05
Minimum = -0.018

Figure 4. Similar to Figure 3, but computed by GEOSIM in mode 5 (fully non-linear) with waves 5, 10, and 15 included.

were similar to the previous works. The discrepancy between our single wave case and that of Quon is left unexplained.

## C. Vacillation

Wave amplitude vacillation is characterized by a periodic growth and decay of a baroclinic wave with a similar periodic decrease and increase of azimuthal mean baroclinicity. GEOSIM in mode 5, with wavenumbers 1 through 15, was run using the same geometric and dynamic parameters as one of the experiments of Buzyna et al. [9]. Figure 5 shows the time variations of kinetic energy integrals for the axisymmetric and wave components in about two vacillation cycles after 21,400 seconds (or approximately 600 rotations) of model integration time. As observed in the laboratory, wave 4 dominates after the system equilibrates to a steady vacillation. Wavenumber 8 and higher harmonics are present, but there is no side-band contribution to the energy spectrum. The period of vacillation is estimated to be 45 rotations, which is two-thirds of what was seen in the laboratory experiments. Figure 6 shows the temperature distributions of the symmetric state and wavenumber four disturbances at the middle level of the model fluid. The four diagrams represent the synoptics at the four phases of a wave amplitude vacillation cycle, denoted by WL, SH, WH, and SL. About 0.3 °C difference in temperature variation between a lowest wave (WL) and a highest wave (WH) stage can be detected, in reasonable agreement with the observations. The movement of the arrow mark indicates that waves travel around the annulus at a frequency about two times as fast as the wave amplitude changes, consistent with the experiments. A more detailed analysis of this and other numerical experiments will be presented in a future paper by Lu, Miller, and Butler.

## D. Bottom-Heated Cylindrical Annulus

Laboratory experiments in which a temperature gradient is imposed on the lower surface of a cylindrical annulus have been performed at MSFC. The outer vertical wall of the annulus is also constrained to have a fixed temperature profile, while the upper and inner walls are made of a relatively non-conducting material (Plexiglass). Many of the results of these experiments are similar to those with the more traditional, side-heated annulus. For example, a boundary representing the transition between stable, axisymmetric flow and that with baroclinic instability in thermal Rossby number-Taylor number parameter space has a similar shape to the side-heated and -cooled experiments. The model was used to predict the transition curve, including number of the initial waves. Figure 7 shows the comparison between the laboratory experiments and the calculated transition. The agreement in placement of the transition curve is fair, but it is not as good as a similar comparison in the side-heated and -cooled case. The agreement in terms of wavenumbers is excellent. The authors believe that the differences in the placement of the transition curve is due to imperfect thermal boundary conditions in the experiment. Significant improvement from a previous comparison was obtained by adding more insulation to the apparatus in the laboratory experiments.
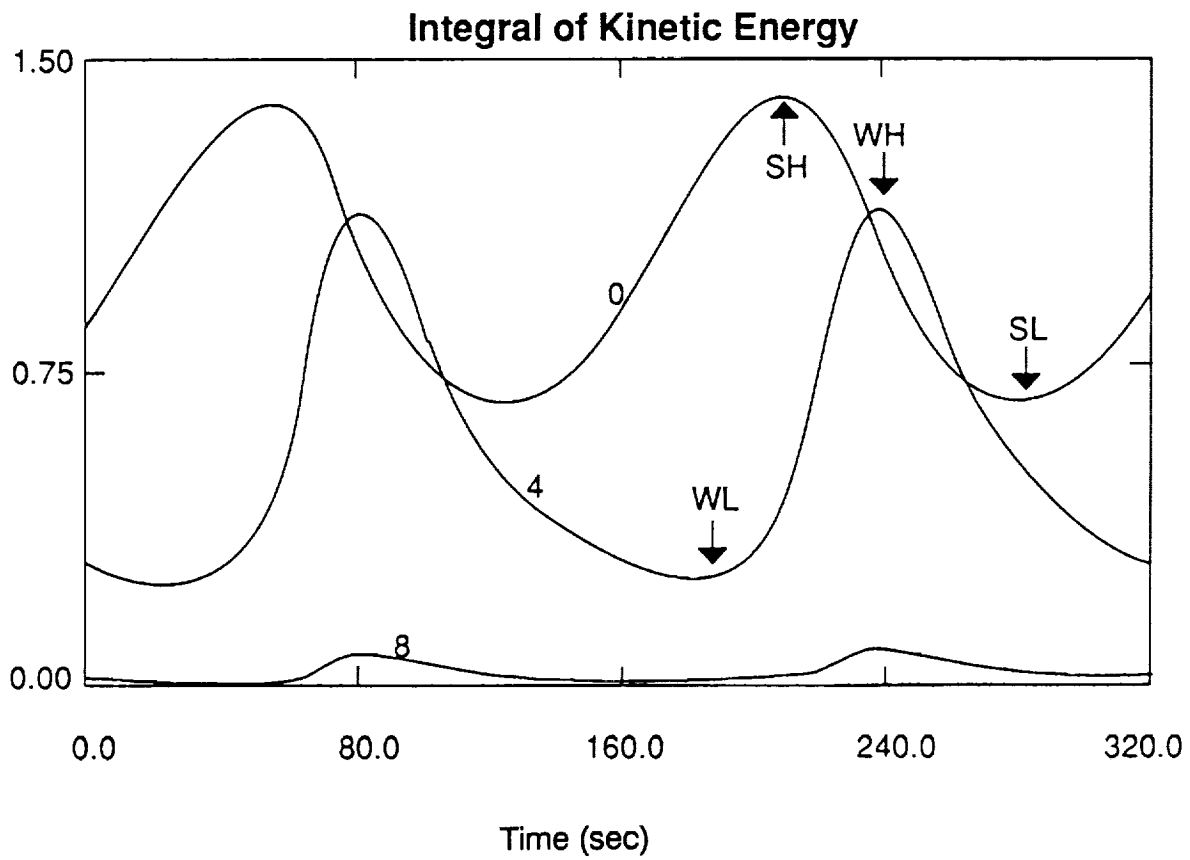
15

# Integral of Kinetic Energy



Figure 5. Time variations of kinetic energy integrals for the axisymmetric and wave components as calculated by GEOSIM for a vacillating case of Buzyna et al. [9], see case B-j of Pfeffer et al. [19].
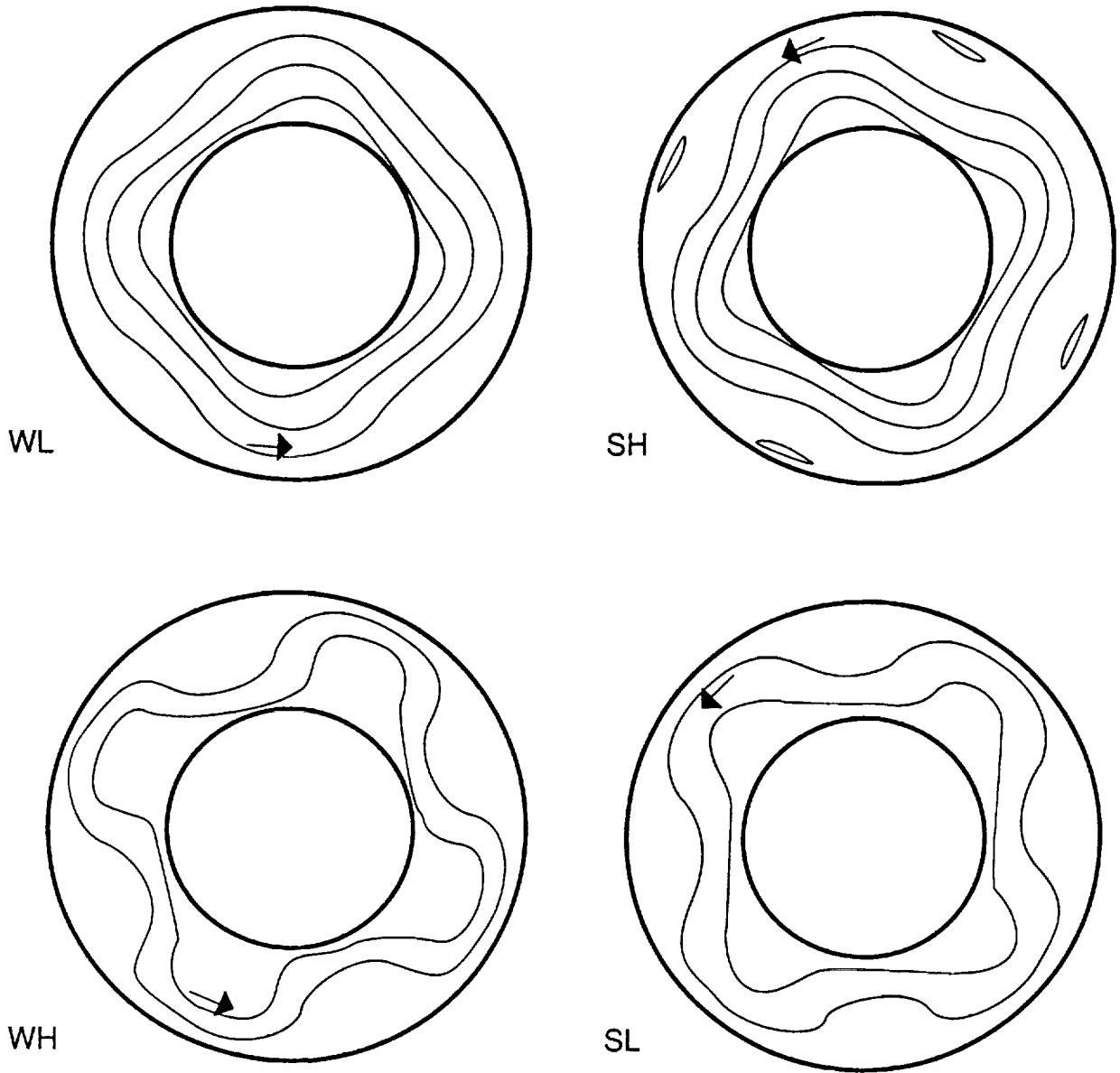
16

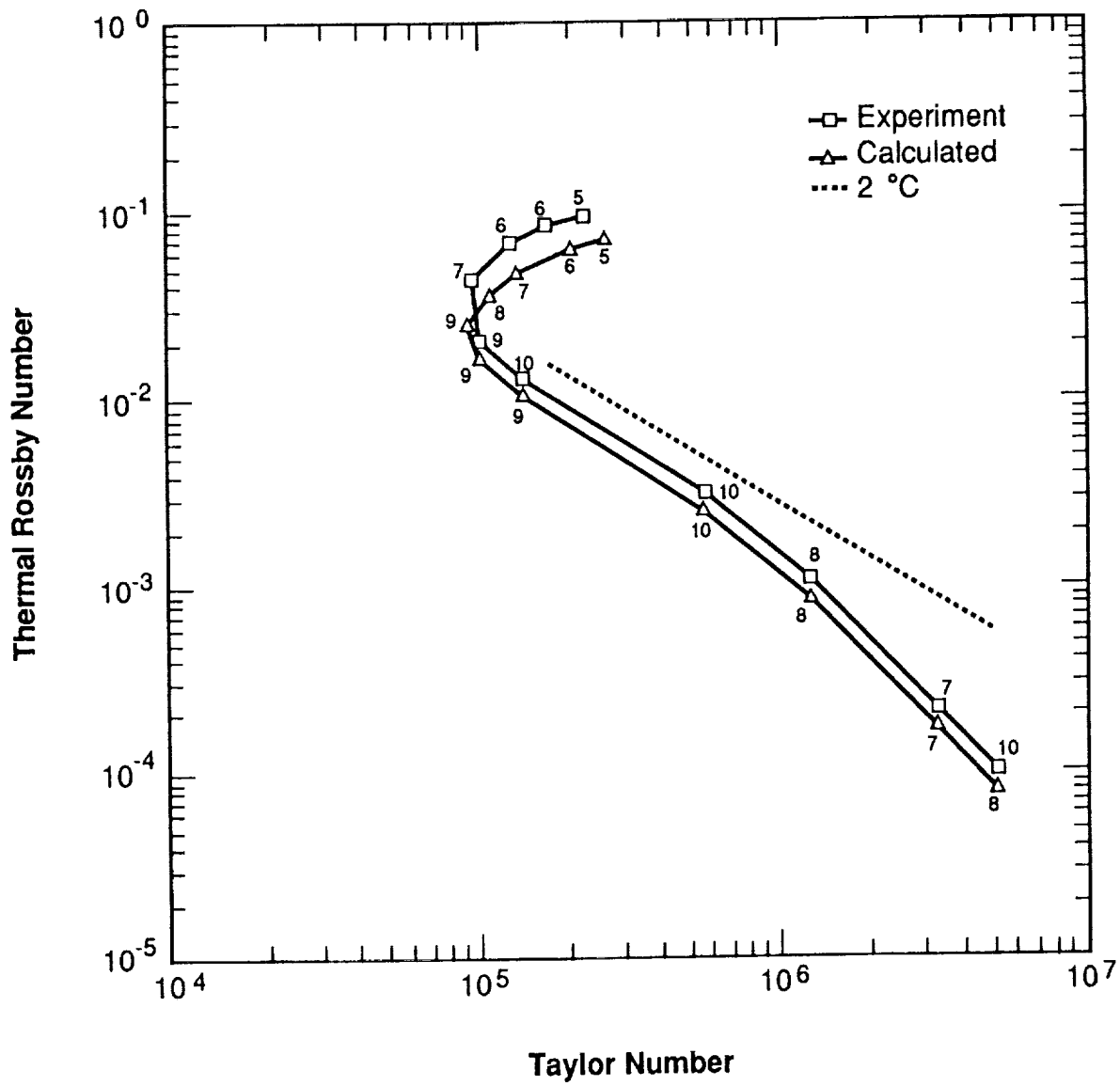Figure 6. Temperature distributions at mid-depth of the annulus for the same case as Figure 5.

Figure 7. Calculated and experimental transitions for the bottom-heated annulus of Miller and Reynolds [10].

## E. Spherical Shell

Comparisons have been made of fully three-dimensional flow patterns predicted by the model with experiments performed on the Spacelab 3 mission with the Geophysical Fluid Flow Cell (GFFC). Agreement was excellent to the extent that the experimental data allow comparison (which is limited to flow patterns). Documentation of these comparisons will appear in a separate paper by Miller and Leslie. More detailed comparisons can be made between the present model and another one, namely a model based on spherical harmonics developed by Gary Glatzmaier of Los Alamos National Laboratory [18]. Note that the Los Alamos model is constrained to have a free-slip condition at the equatorial wall, so the present model was run with that condition as well. An initial condition was determined by integrating the Glatzmaier model for a short time (see Figures 8 and 9). The fields at that point were then used as initial conditions for both models. After 9 minutes, the results from the two models are compared in Figures 8 and 9 for temperature and for radial velocity at mid-depth. Note that the agreement is remarkable, in spite of the fact that the patterns have changed significantly from the initial conditions. Further comparisons are in progress for a case with stronger gravity, in which the fields change more quickly and in which the results have been shown to be extremely sensitive to initial conditions. These comparisons will be published separately by Johnston and Miller.

## IV. SUMMARY

The MSFC-developed model GEOSIM has been shown to be an extremely powerful tool for simulating a wide range of geophysical flow problems. The model employs finite differences in the meridional plane and spectral decomposition in the azimuthal direction, which results in a code which is flexible in terms of domains and boundary conditions. The use of a spectral transformation in the azimuthal direction allows the calculation of axisymmetric states, linear waves, and states with wave-mean flow interaction only. The code has been validated by comparing its results to both experimental and numerical studies. The example cases that are given in this paper demonstrate the types of fluid flow problems which GEOSIM was designed to solve. Further research at MSFC using the model is planned, and the authors welcome inquiries from researchers with similar needs and interests who may wish to use the model.
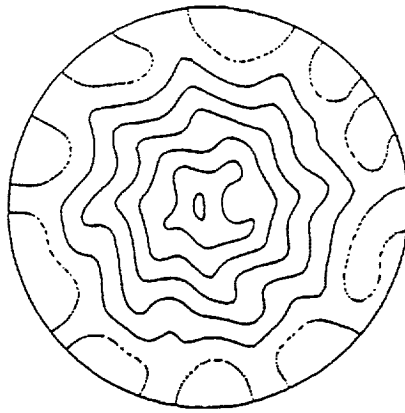
TEMPERATURE AT     2.78 CM          MAXIMUM =  10.17
CONTOUR INTERVAL =      2.0          MINIMUM =  -3.90
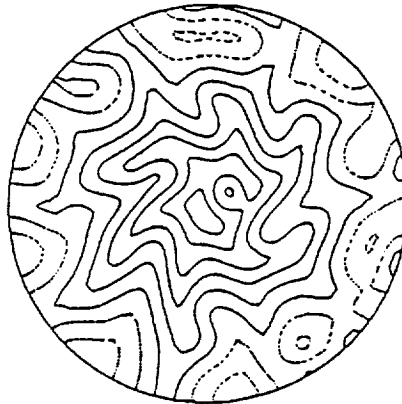


TEMPERATURE AT     2.78 CM          MAXIMUM =  11.08
CONTOUR INTERVAL =      2.0          MINIMUM =  -5.37
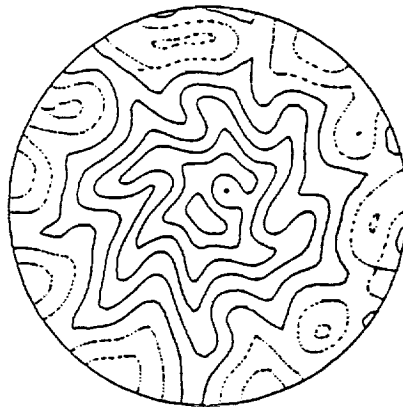


TEMPERATURE AT     2.78 CM          MAXIMUM =  11.03
CONTOUR INTERVAL =      2.0          MINIMUM =  -5.34

Figure 8. Temperature fields from the comparison between GEOSIM and the model of
Glatzmaier [18]. The upper plot is that of the initial condition (same for both models). The
middle plot is from the GEOSIM model 9 minutes later, and the lower plot is from the
Glatzmaier model at the same time.
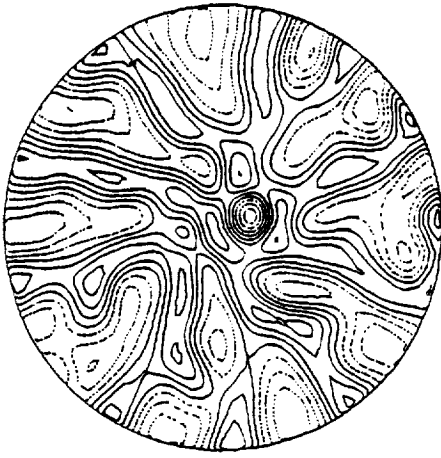
VERTICAL VELOCITY AT 2.78 CM        MAXIMUM = 0.0087
CONTOUR INTERVAL =        0.002        MINIMUM = -0.0082
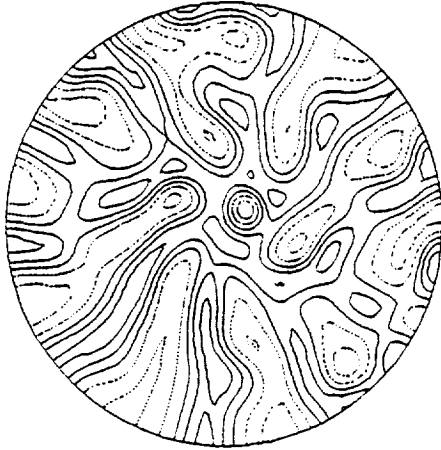
VERTICAL VELOCITY AT 2.78 CM        MAXIMUM = 0.016
CONTOUR INTERVAL =        0.005        MINIMUM = -0.014

VERTICAL VELOCITY AT 2.78 CM        MAXIMUM = 0.016
CONTOUR INTERVAL =        0.005        MINIMUM = -0.015

Figure 9. Similar to Figure 8, but for radial velocity component.

# REFERENCES

1. Fein, J. S., An experimental study of the effects of the upper boundary condition on the thermal convection in a rotating, differentially heated cylindrical annulus of water, Geophys. Fluid Dyn., 5, 213-243 (1973).

2. Pfeffer, R. L., G. Buzyna, and R. Kung, Time-dependent modes of behavior of thermally-driven rotating fluids, J. Atmos. Sci., 37, 2129-2149 (1980).

3. Hart, J. E., G. A. Glatzmaier, and J. Toomre, Space-laboratory and numerical simulations of thermal convection in a rotating hemispherical shell with radial gravity, J. Fluid Mech., 173, 519-544 (1986).

4. Miller, T. L., and R. L. Gall, Thermally driven flow in a rotating spherical shell: Axisymmetric states, J. Atmos. Sci., 40, 856-868 (1983).

5. Miller, T. L., and R. L. Gall, A linear analysis of the transition curve for the baroclinic annulus, J. Atmos. Sci., 40, 2293-2303 (1983).

6. Miller, T. L., and K. A. Butler, A numerical study of the transition between axisymmetric flow and wave flow in the baroclinic annulus, including hysteresis, J. Atmos. Sci., in press (1991).

7. Miller, T. L., and J. D. Fehribach, A numerical study of the onset of baroclinic instabilities in spherical geometry, Geophys. Astrophys. Fluid Dyn., 52, 25-43 (1990).

8. Williams, G. P., Baroclinic annulus waves, J. Fluid Mech., 49, 417-449 (1971).

9. Buzyna, G., R. L. Pfeffer, and R. Kung, Kinematic properties of wave amplitude vacillation in a thermally driven rotating fluid, J. Atmos. Sci., 46, 2716-2729 (1989).

10. Miller, T. L., and N. D. Reynolds, A laboratory and numerical study of baroclinic instability in a cylindrical annulus with the temperature gradient imposed on the lower surface, J. Fluid Mech., submitted (1991).

11. Quon, C., A mixed spectral and finite difference model to study baroclinic annulus waves, J. Comp. Phys., 20, 442-479 (1976).

12. McChenhauer, B., The spectral method in numerical methods used in atmospheric models, Vol. II, GARP Publication Series No. 17, World Meteorological Organization, 1979.

13. Roache, P.J., On artificial viscosity, J. Comp. Phys., 10, 351-366 (1972).

14. Warn-Varnas, A., W. W. Fowlis, S. Piacsek and S. M. Lee, Numerica solutions and laser-Doppler measurements of spin-up, J. Fluid Mech., 85, 609-639 (1978).

15. Williams, G. P., Numerical integration of the three-dimensional Navier-Stokes equations for incompressible flow, J. Fluid Mech., 37, 727-750 (1969).

16. Sweet, Roland A., A parallel and vector variant of the cyclic reduction algorithm, SIAM J. Sci. Stat. Comput., 9, 761-765 (1988).

17. Temperton, C., A note on prime factor FFT algorithms, J. Comput. Phys., 52, 198-204 (1983).

18. Glatzmaier, G. A., Numerical simulation of stellar convective dynamics. Part I: The model and method, J. Comp. Phys., 55, 461-484 (1984).

19. Pfeffer, R. L., G. Buzyna, and R. Kung, Time-dependent modes of behavior of thermally-driven rotating fluids, J. Atmos. Sci., 37, 2129-2149 (1980).

APPENDIX A: User's Guide

The current version of the GEOSIM model (1990) was developed and runs on the CRAY XMP at Marshall Space Flight Center (MSFC). While this User's Guide often specifically refers to the Cray, we have generally avoided using instructions that are unique to this machine. With the construction of proper operating system commands, the model should run at any site that supports a FORTRAN 77 compiler. For example, it has been successfully run on an IBM RISC 6000.

### Compilation Procedures

The model's source code is contained in four ASCII files: one for the main program and subroutines, one for subroutines used in the FFT and the elliptic equation solver, one for the derived parameter statements and common blocks, and one for the key parameter statements. The file with the common blocks is "included" in the main program and most of the subroutines at the time of compilation. The sizes of the work arrays are set by the user to the desired value in the key parameter statements. In the current implementation on the Cray, these parameter statements are in the same file as the operating system commands that compile the code. Note that, while the radial and latitudinal grids used must be the same as the array dimensions, the number of waves can be less than or equal to the compiled dimension. The following key parameters must be set at compilation:

MIIW:     Maximum number of wave components (excluding the axisymmetric component)

JJ:       Number of grid points in the meridional direction. Note that the number of interior grid intervals in JJ - 2.

KK:       Number of grid points in the vertical direction. The number of interior grid intervals is KK - 2.

NONCASE:  Selection for mode of operation (determines whether FFT is used).
          = 1: Fully nonlinear run
          = 0: Any other mode of operation

IWDIM:    Dimension of the work array for the elliptic equation solver. A formula is given for estimating the minimum value of this parameter. If the value is too small, an error message is printed and the model does not run.

### Restart Files and Restart Procedure

At the end of each integration, each wave component (excluding the axisymmetric part) is written to a separate logical unit (7 and above), and all waves are concatenated and written to a single logical unit (99). (Only one of these sets of files--whichever is more convenient for the user--needs to be saved.) The axisymmetric data contain grid information, are slightly different in format from the wave data, and are written to logical unit 1. The user can choose to save

25

whichever files desired for analysis and/or restarting the model. There are several ways to initialize the model:

ISTART = -2: Restart from scratch - This uses boundary temperature and profile information within the source code to set up the initial axisymmetric temperature field. (The interior temperature field can either be a constant value or an interpolation of the boundary values. This is determined by the input parameter "TINIT," which is on the last line of the input deck.) If waves are included, they are initialized with a small temperature disturbance (randomly oriented in the azimuthal direction) located in the middle of the meridional grid.*

ISTART = -1: Axisymmetric restart - A previously computed axisymmetric field on unit 1 (with grid information) is used as an initial condition. The waves are initialized in the same way as a "scratch" run.

ISTART = 1: Both axisymmetric and wave fields are read from units 1 and 7 (and up, if necessary), respectively. Note that the wave fields must be in ascending order

---

*There is a call to the random number generating routine RANF in the subroutine INITIA. This is a spot where the user may need to make a change for a different computer installation.

Input Parameter File

The unit 5 input file (usually concatenated with the operating system commands to run the model) prescribes various numerical and physical parameters necessary to run the model. Table A.1 defines each of the input parameters. The grid and boundary temperature parameters are used only in the "scratch" starts; other parameters are used in all run modes and replace any values stored in the axisymmetric save file. For example, if an axisymmetric field is run with omega = 2.0 and restarted with omega = 1.8 in the runstream, the value of 1.8 is used in the new run. Unless a "delta omega" of -0.2 is input, the model does not add the differential spin-up rotation; that is, the u-field in the input file is taken to be relative to the new rotation rate. Boundary conditions on temperature cannot be changed in a restart. (It would be straightforward for the user to write a program which edits the restart file to change them, if desired.)

Diagnostics such as integrated kinetic energy are calculated at intervals.which depend on the "NSTEP" and "ISKIP" factors. If the number of steps (NSTEP) is set to 5000 and the skip factor (ISKIP) is set to 1000, diagnostics.are be written to the output file on steps 0,1,1000,2000...,5000. If ISKIP is set to zero, the default factor of NSTEP/200 is used for ISKIP, and therefore the diagnostics are written 202 times. A summary page, which contains basic information for the axisymmetric state and all of the waves, is written after every 5 pages of diagnostics.

The "IRUNCD" option corresponds to the mode of integration that is to be run in the model. A "1" indicates an axisymmetric only run, "2" - linear waves only, "3" - axisymmetric and linear waves (no interaction), "4" - axisymmetric and nonlinear wave (wave-mean flow interaction), and "5" - fully nonlinear wave run. The value of IRUNCD affects the interpretation of the "WAVE-NUMBERS" line. In modes 2 through 4, this refers to the wavenumbers included in the calculations. In mode 5, this line lists the waves to be included in the printed diagnostic output, the "WAVE FACTOR" indicating which set of wave numbers to run. For example in mode 5, if the number of waves is set to 10 and the wave factor is set to 3, then waves 3,6,9...30 would be included in the calculation. Table A.2 gives a list of memory and time requirements for each run option for both cylindrical and spherical example runs.

The boundary conditions are defined by the values of "IBTMP" (temperature) and "IFREE" (u,v,w components). Both IBTMP and IFREE are arrays of four elements which correspond to the four sides of the grid. A heated wall or a no-heated wall are specified by setting the respective IBTMP to -1 or 1. Similarly, for rigid or free walls, set IFREE to either -1 or 1. The values of IFREE and IBTMP do not influence polar conditions for the computations, although to obtain good plots they should both be set to 1.

Printed output and plots

Selected output is sent to unit 6. The majority of the input stream is written within the first 2 pages. After that, diagnostics for the axisymmetric field are given (if not running in IRUNCD = 2 mode), and then the waves are written (one per page). Diagnostics include

27

Table A.1. GEOSIM Input File Definitions.

| Parameter | Definition |
|---|---|
| NSTEP | Number of time steps |
| ISKIP | Skip factor for diagnostics (leave zero for default value of diagnostics calulated 202 times) |
| IRUNCD | Mode of model integration |
| IBTMP | Temperature boundary conditions |
| IFREE | Momentum boundary conditions |
| IPROF | Profile for initial horizontal temperature gradient |
| COND | Thermal diffusivity |
| VISC | Kinematic viscosity |
| EXPAN | Thermal expansivity |
| OMEGA | Rotation rate |
| DOMEG | Used for spin-up cases |
| DELT | Time step |
| DTFAC | Time step factor for temperature |
| AXIFAC | Time step factor for the axisymmetric part |
| GAMT | Optional ADI for temperature (zero for ADI, one otherwise) |
| GAMV | Optional ADI for velocities (same comment) |
| RMAX | Maximum divergence residual (criterion for pressure correction) |
| ICONV | Wave convergence parameter |
| ISTART | Restart option |
| PHI1 | Lower meridional boundary (degrees for spherical cases, radians for cylindrical) |
| PHI2 | Upper meridional boundary (same comment) |

Table A.2. Memory and Time Requirements for Typical GEOSIM Integrations.

|  | Symmetric only | Linear | Wave/Mean flow | Nonlinear (1 wave) | Nonlinear (15 waves) |
|---|---|---|---|---|---|
| Option | 1 | 2 | 4 | 5 | 5 |
| 30X30 grid | 0.39 (62) | 0.44(127) | 0.44 (223) | 0.46 (229) | 1.26 (2170) |
| 50X20 grid | 0.32 (65) | 0.35(135) | 0.35 (238) | 0.38 (245) | 1.25 (2429) |

The first number indicates memory requirements in CRAY megawords. The number in parenthesis is the number of seconds that were required to run 5000 time steps.

integrals of such quantities as kinetic energy, heat fluxes, and energy conversions. The user is referred to the subroutines beginning with DIAG... for the definitions of the diagnostics.
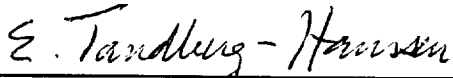
A plot routine (separate from the model) runs on the IBM front-end, is menu driven, and plots cross sections of fields (either total or components) in any one of three planes. It also allows viewing of certain integrated diagnostics, plotted as a function of time. Because it is unlikely that a potential user would be able to transport this code to a different installation, documentation is not given here.

# APPROVAL

## GEOSIM - A Numerical Model for Geophysical Fluid Flow Simulation

### By  Karen A. Butler, Timothy L. Miller, and Huei-Iin Lu

The information in this report has been reviewed for technical content.  Review of any information concerning Department of Defense or nuclear energy activities or programs has been made by the MSFC Security Classification Officer.  This report, in its entirety, has been determined to be unclassified.

E. TANDBERG-HANSSEN
Director
Space Science Laboratory